J. Komori[1], R. Ando[2], S. Miura[3], and R. Arai[3]

[1]Earth Observatory of Singapore, Nanyang Technological University, 50 Nanyang Avenue, Singapore.

[2]Department of Earth and Planetary Science, School of Science, University of Tokyo, 7-3-1 Hongo, Bunkyo-ku, Tokyo, Japan

[3]Research Institute for Marine Geodynamics, Japan Agency for Marine-Earth Science and Technology, 3173-25, Showa-machi, Kanazawa-ku, Yokohama, Kanagawa, Japan

Corresponding author: Junki Komori (junki.komori@ntu.edu.sg)

Key Points:

- Simulated deformation history around the Sagami Trough using mechanical subduction model
- The kinematic back-slip model is not suitable for investigating earthquake cycles
- A subducted seamount plays a significant role in the crustal uplift at the southernmost Boso Peninsula.

Abstract

We developed a mechanical subducting plate model and re-examined the crustal deformation history in the Sagami Trough subduction zone, central Japan, the northernmost convergence boundary of the Philippine Sea Plate. The elevation distributions and formation ages of the Holocene marine terraces, representing past coseismic and long-term coastal uplifts, have been thoroughly investigated in this region. However, no physically consistent formation scenario to explain them has been demonstrated. Surface deformations within subduction zones are typically calculated using kinematic elastic dislocation models, such as the back-slip model. However, these models cannot explain permanent deformation after an earthquake sequence. This study develops a mechanical subducting plate model that balances the slips of interplate shear stress and can produce permanent deformations caused by a local bump geometry. We modeled earthquake recurrences by shear stress accumulation and coupling patches. As a result, we successfully reproduced the averaged uplift rate distribution estimated from the Holocene marine terraces. The findings suggest that the subducted seamount significantly affects long-term deformation patterns. In addition, the discrepancy between the elevation distributions and formation ages of Holocene marine terraces, which previous geological studies have indicated, can be interpreted by the rupture delay of coupling patches. This study also demonstrates that the traditional assumption of the back-slip model on the plate boundary for long-term subduction possibly results in an oversimplified model.

Plain Language Summary

Marine terraces are stair-like coastal landforms that can be seen in the regions where the land is uplifting. Four levels of marine terraces in the southernmost part of the Boso Peninsula, central Japan, are considered to have been uplifted by past great earthquakes. Therefore, it is important to understand how these terraces were created for estimating future earthquakes. However, it has been difficult to explain by using a computational model. This study created a new earthquake and deformation model and investigated the terrace formation process. We focused on the force balance, not balance of slip, in this new model. The findings suggest that a sea-floor volcano squeezed in the plate boundary plays an important role in the formation and uplifts of the terraces. In addition, the traditional "characteristic earthquake model," which is a repeat of the same slips with constant intervals, cannot explain the geological and geomorphological observations.

1 Introduction

Understanding fault rupture patterns is critical for future hazard assessment. However, the typical recurrence interval of subduction earthquakes exceeds a century, and it may take longer than thousands of years to complete a recurrence pattern (so-called "earthquake supercycles") (Grant and Sieh, 1994; Philibosian and Meltzner, 2020). Because modern instrumental observation only records up to a century of history, we rely on historical and geological records to elucidate the fault rupture history.

Marine terraces are characteristic coastal landforms recognized as geological records of past crustal uplifts (Keller and Pinter, 2002). Multiple levels of Holocene terraces are, in general, regarded as a clue for the past rupture recurrence around subduction zones (Shimazaki and Nakata, 1980; Ramos and Tsutsumi, 2010; Wang et al., 2013; Litchfield et al., 2020). However, studies interpreting the rupture history from Holocene terraces frequently use the average uplift rates and a simple extrapolation of the latest or well-observed seismic event. Few studies have discussed terrace formation and development relying on a physically consistent crustal deformation model over earthquake sequences (e.g., Sato et al., 2016). An interpretation based on a simplified model with insufficient kinematic and mechanical reasonableness may overestimate and underestimate future hazards. Therefore, it is critical to develop a crustal deformation model around subduction zones, including earthquake recurrences, and re-examine rupture histories.

The crustal deformation around subduction zones is commonly explained using a kinematic model based on the dislocation in an elastic half-space. In particular, the back-slip model of Savage (1983) is frequently used to interpret the deformation during the interseismic period. This model approximates the source of interseismic deformation as an opposite direction slip deficit (back-slip) on the interplate coupling area. This model reasonably reproduces the snapshots of interseismic surface deformation and is useful for geodetic inversion, which estimates the locations and magnitudes of interplate couplings (Yoshioka et al., 1993; Nishimura et al., 2004). However, given that the coseismic slip amount is

equivalent to the accumulated slip deficit during the interseismic period, the net crustal deformation will be canceled out after an earthquake cycle. Thus, the formation of marine terraces has not been explained by the simple kinematic earthquake cycle model because it predicts that the uplifted coast will return to sea level before the next event.

Sato and Matsu'ura (1988) explained the permanent uplift around a subduction zone by developing a kinematic plate-subducting model in an elastic/viscoelastic half-space. By assuming that the interseismic back-slip cancels out the coseismic forward slip, they demonstrated that the forward slip at the subduction rate on the curved plate interface could produce permanent deformation in the overriding plate with gravitational compensation (Matsu'ura and Sato, 1989; Fukahata and Matsu'ura, 2016). They emphasize the role of the steady-rate forward slip in predicting the steady uplift and posited the effect of the coseismic (intermittent) uplift on the marine terrace formation is insignificant.

Kanda and Simons (2010) proposed another kinematic subduction model in an elastic half-space that produces permanent uplift. While the back-slip model approximates interseismic coupling as the slip deficit in a seismogenic zone, their model (named elastic subducting plate model (ESPM)) provides steady slips to the decoupled areas on the upper and lower interfaces of the subducting plate. This configuration simulates a more realistic feature of a subduction zone with one additional free parameter (thickness of the plate) than the back-slip model. The ESPM also produces permanent uplifts after an earthquake cycle because of the bending of the subducting plate.

Kinematic earthquake recurrence models typically determine the magnitude of a coseismic slip to compensate for the slip deficit (back-slip) amount during the interseismic period. However, this assumption is not necessarily physically reasonable because the accumulated shear stress should drive the fault rupture, not the slip deficit. Shear stress accumulation also depends on the local geometry if stress changes affected by the slip outside the rupture area are considered. Therefore, the compensation of stress changes does not always imply a cancel out between coseismic slip and interseismic back-slip. This study proposes a mechanical earthquake recurrence model focusing on these differences in the boundary condition.

The mechanical constraint on the fault slip and back-slip distributions has been used for geodetic inversion studies (Johnson and Segall, 2004; Johnson and Fukuda, 2010; Herman et al., 2018; Herman and Govers, 2020; Lindsey et al., 2021). Conventional geodetic inversions employ smoothing parameters over the slip distribution to obtain steady results. However, such a constraint was not physically supported and might have overlooked the potentially seismogenic fault (Lindsey et al., 2021). The mechanical constraint inversion detects coupling patches on the plate interface and predicts physically reasonable slip distributions. This study develops a crustal deformation model using such a coupling patch concept for earthquake recurrences.

Moreover, this study focuses on the effect of a subducted seamount on long-term surface deformation. Various studies on the long-term deformation around subduction zones, such as analog experiments (Dominguez et al., 1998; 2000), geological observations (Gardner et al., 2001), and numerical model simulations (Litchfield et al., 2007), have discussed the relationship between them. However, few studies on Holocene marine terraces have considered this relationship. Although the effect of the interplate geometry in each earthquake event is small, it is not negligible when we discuss the deformation accumulation for thousands of years.

We examine the deformation history around the Sagami Trough subduction zone for the past 6,000 years using the newly proposed mechanical earthquake recurrence model. Four levels of Holocene marine terraces, which are thought to have been uplifted by megathrust earthquakes, are distributed in the southernmost part of the Boso Peninsula, which is approximately 30 km to the north of the Sagami Trough axis. These terraces are named Numa terraces (Nakata et al., 1980), and their elevation distributions and formation ages have been accurately estimated by our recent geological investigations (Komori et al., 2017; 2020; 2021). The recurrence history of the megathrust earthquakes here is also of significant interest from a disaster mitigation viewpoint because of the proximity of the Tokyo metropolis. The purpose of this study is to use a single comprehensive subduction model to explain the coseismic uplift, interseismic deformation, and long-term displacement, including multiple earthquake sequences, i.e., the current elevation distributions of the Numa terraces.

2 Tectonic setting and geological observations

The Sagami Trough is a convergence plate boundary, where the Philippine Sea Plate (PHS) subducts north-westward beneath the continental plate of northeast Japan (Figure 1a). This subduction zone exhibits a remarkably complex geometry; the triple junction, where the Pacific Plate subducts below the PHS, and the Izu Peninsula, a collided volcanic island, mark the eastern and western ends, respectively. Historical documents record two interplate earthquakes along this plate boundary: the 1703 M8.2 Genroku Kanto earthquake and the 1923 M7.9 Taisho Kanto earthquake (hereafter, the 1703 Genroku earthquake and the 1923 Taisho earthquake, respectively) (Usami et al., 2013). The 1923 Taisho earthquake uplifted the coastal area by approximately 2 m around Sagami Bay. Furthermore, the uplifted coast records approximately 6-m vertical displacement at the southernmost tip of the Boso Peninsula caused by the 1703 Genroku earthquake.

Various geological and geomorphological studies have investigated the Numa terraces for a long time (Watanabe, 1929; Matsuda et al., 1978; Nakata et al., 1980; Kawakami and Shishikura, 2006) (Figure 1b). The four levels of the Numa terraces are numbered as Numa I, II, III, and IV in descending order (Nakata et al., 1980). Based on historical documents, the lowest one, Numa IV, is regarded as the preserved uplift caused by the 1703 Genroku earthquake.

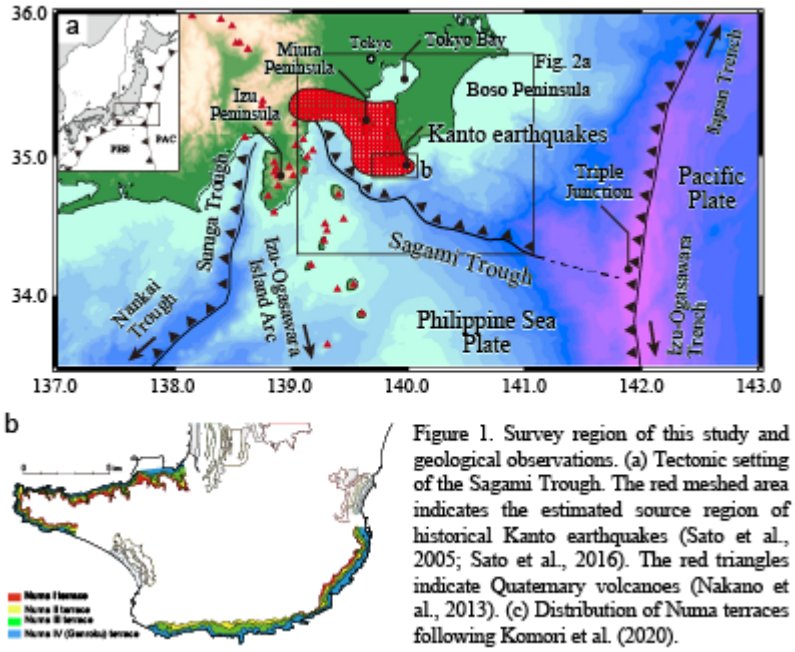

Figure 1. Survey region of this study and geological observations. (a) Tectonic setting of the Sagami Trough. The red meshed area indicates the estimated source region of historical Kanto earthquakes (Sato et al., 2005; Sato et al., 2016). The red triangles indicate Quaternary volcanoes (Nakano et al., 2013). (c) Distribution of Numa terraces following Komori et al. (2020).

From the similarity in the distribution of these terrace platforms, the Numa terraces are thought to be records of similar type >M8 class megathrust earthquakes (Genroku-type earthquakes). In our previous investigation, we dated their ages from buried shell fossils to approximately 5,730 yBP, 3,270 yBP, 2,000 yBP, and CE1703 (the Genroku earthquake) in descending order (Komori et al., 2021). Furthermore, we indicated that the relative height of each level is similar; it marks more than 6 m at the southernmost tip and steeply decreases toward the north (approximately 3 m per 10 km) (Komori et al., 2020).

On the other hand, the recurrence of earthquakes such as the 1923 Taisho earthquake is also assumed, which does not cause Numa terrace class uplift but occurs more frequently. Shishikura et al. (2001) found that the western coast of the Boso Peninsula had experienced a few meters of uplift every 400 to 1,000 years in the past 7,000 years by investigating the beach ridges. Besides, an investigation of tsunami deposits reported that this region had suffered tsunamis comparable to the 1923 event every 100 to 300 years (Fujiwara et al., 2000). Considering that these tsunami deposits do not always imply Sagami Trough events and that the beach ridges are not always preserved, smaller Taisho-type events may occur at 200–400-year intervals (Shishikura, 2014).

Previous studies have also discussed the formation scenario of the Numa terraces and the occurrence history of the Kanto earthquakes. Earlier studies (e.g., Matsuda et al., 1978) correlated the Numa terrace distribution with the pattern of the coseismic uplift and interseismic subsidence for historical earthquakes. However, the similarity in the spatial distribution of these terraces has

not been simply thought to evidence the recurrence of the characteristic earthquakes. Sato et al. (2016) demonstrated that permanent uplifts caused by the plate subduction possibly remain at the southernmost Boso using the kinematic formula in an elastic/viscoelastic half-space (Sato and Matsu'ura, 1988). However, they also indicated that the long-term deformation is approximated to be a steady motion and that the formation of the Numa terraces is not related to the Kanto earthquakes, except for Numa IV. Noda et al. (2018) explained the current elevation distributions of the Numa terraces by combining the steady uplift and sea level fluctuations, generally applied to late-Pleistocene marine terraces. This model anticipated that the Numa terraces have a reversal formation age (i.e., a higher terrace is younger than a lower terrace) at some part; however, subsequent geological studies (Komori et al., 2020; 2021) have not found such a feature.

In addition, previous studies have highlighted several discrepancies between uplift patterns expected from existing models and the geological observation of the Numa terraces. First, the characteristic wavelength for the permanent uplift caused by the plate subduction is greater than 100 km because the deformation is controlled by the bending of the subducting plate, whether with the elastic/viscoelastic model (Sato et al., 2016) or ESPM (Kanda and Simons, 2010). However, we have discovered that the elevation of the Numa terraces steeply decreases by 10 to 20 km for each level in our previous geomorphological study (Komori et al., 2020). Besides, kinematic models expect a linear relationship between the formation ages and the present elevation of these terraces. The dating results also oppose this prediction that the Numa terraces have similar relative heights but variable formation intervals of up to twice as long (Komori et al., 2021).

This study discusses the relationship between the permanent uplift and the plate interface geometry. Several previous reflection surveys have investigated the tectonic structure around the Sagami Trough subduction zone and the geometry of the upper interface of the PHS. Figure 2a depicts the profiles of these previous surveys (Sato et al., 2005; Kimura et al., 2009; Miura et al., 2009; Tsumura et al., 2009). Past geological studies conducted in other regions have reported subducted seamounts and inland faults branching from the main thrust as possible causes of permanent deformations around subduction zones (Plafker et al., 1969; Gardner et al., 2001; Litchfield et al., 2020). Here we confirm the tectonic setting of the study region from previous investigations and estimate the possible cause of the permanent uplift in the Boso Peninsula. Tsumura et al. (2009) conducted a series of surveys in the nearest shore region to this survey region (Figure 2a) and reported the existence of a subducted seamount. In addition, Miura et al. (2009) obtained another cross-section in the southeast offshore Boso (Figure 2b), which crosses the multiple survey lines of Tsumura et al. (2009). Comparing them in the migrated time sections (see Figure 7 in Tsumura et al. (2009)), the positions of the reflectors are comparable at the cross points. Therefore, these two independent surveys strongly suggest an irregular geometry, possibly a subducted seamount beneath the southernmost part of the Boso

Peninsula. Considering the tectonics in this subduction zone (Figure 1a), this subducted seamount is likely a part of the Izu-Ogasawara Island Arc.

No obvious activity of intraplate faults in the upper plate is confirmed in the surrounding region of this study area. In the central part of the Boso Peninsula, approximately 20 km north of the study area, an active fault zone (Kamogawa-teichi fault zone) is recognized but shows no clear geological record of activities in the late Quaternary (Komatsubara, 2017). Kimura et al. (2009) discovered several splay faults branching from the main thrust in the offshore region. However, the branching faults in the shallower part, which likely form Boso Canyon at the seafloor, do not connect to other reflection survey results in the west (Miura et al., 2009; Tsumura et al., 2009). This branch fault may have merged with the main thrust, where Boso Canyon meets the Sagami Trough. Another branching fault in the northeast, probably exposed as Katsuura Canyon, connects to the Kamogawa-teichi fault zone judging from the seafloor topography. Therefore, we assume that no intraplate faulting contributes to the crustal deformation in the modeling hereafter.

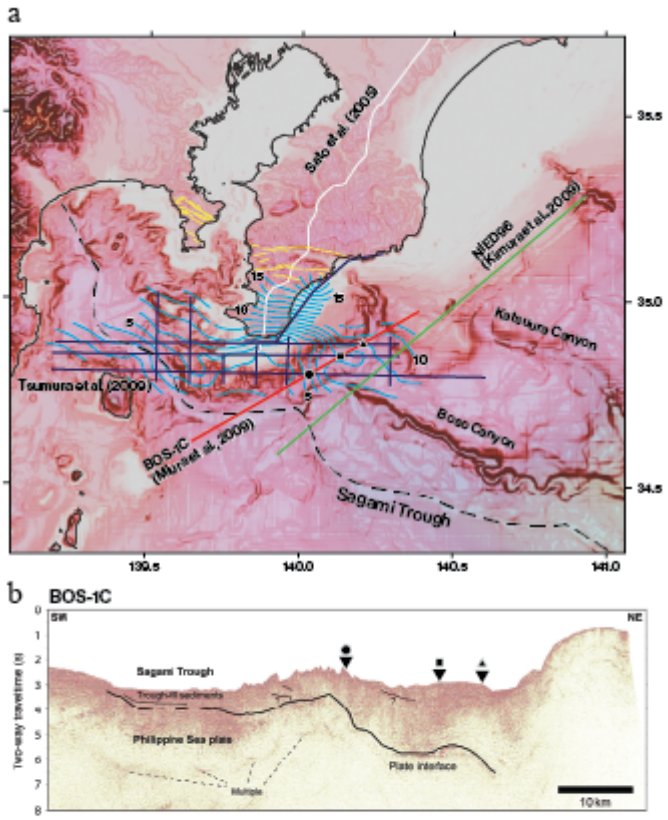

Figure 2. (a) Bathymetry map around the survey region and the profile lines of previous reflection surveys (Sato et al., 2005; Kimura et al., 2009; Miura et al., 2009; Tsumura et al., 2009). The blue contour lines indicate the estimated depth of the upper PHS by Tsumura et al. (2009). (b) Post stack time-migrated reflection image of the BOS-1C profile (Miura et al., 2009). The solid black line represents our interpretation of the plate interface. Triangles indicate the positions of intersections with the survey lines of Tsumura et al. (2009).

3 Models and Methods

We simulate the crustal deformation around the subduction zone using the mechanical dislocation model. In this study, we combine the concepts of the ESPM proposed by Kanda and Simons (2010; 2012) and mechanical coupling (Johnson and Segall, 2004; Herman et al., 2018). Figure 3 schematically depicts the configuration for the plate subduction. First, we set the upper and lower boundaries of the subducting oceanic plate and then divide them into a coseismic slip area and remaining interseismic steady slip zones. If a uniform slip is applied to this coseismic slip area, this setting is consistent with the ESPM. In the interseismic period, the coseismic slip area is further classified into coupling patches and decoupled zones. Thus, the boundary condition for the interseismic period is (1) uniform slips (equivalent to the plate subduction rate) on the steady slip zone,

which are in opposite directions between the upper and lower boundaries, (2) no-slip on coupling patches, and (3) no shear stress change on decoupled zones. Next, we apply coseismic dislocations to compensate for the accumulated shear stress on coupling patches. We can calculate the slip distribution via a linear inversion when coseismic shear stress changes (stress drop) are provided. The detailed formula for this model is in the supplementary material. We can construct a forward model for the earthquake recurrence using the location and size of coupling patches and their rupture timings.

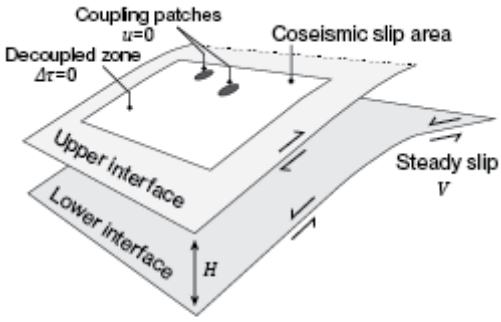

Figure 3. Schematic illustration of the mechanical plate subduction model. The boundary conditions during the interseismic period are displayed in this figure. The steady slip zone is given as a sufficiently large area compared with the coseismic slip area in the model even though it is excluded in this figure.

We modeled the earthquake recurrence along the Sagami Trough and investigated the relationship between the deformation history, the configurations of coupling and rupture, and the plate interface geometry. We have two open questions about the formation of the Numa terraces: the long-term uplift rate and its distribution, and the relative height of the marine terraces, i.e., the total vertical displacements between rupture events. The long-term deformation in this model is, as subsequently demonstrated, independent of the configuration of rupture patches. Hence, we first investigate how the interplate geometry impacts the final deformation pattern. Here, we mainly focus on the contribution from the subducting seamount beneath the survey area (Tsumura et al., 2009) and discuss separately the effect of the complex tectonic geometry of the Sagami Trough (Hashimoto et al., 2004; Sato et al., 2005; Hirose et al., 2008). Therefore, we use two plate boundary topographies that are simpler and more realistic and first investigate the effect of the subducting seamount with a flatter subducting plane.

Next, we investigate how the rupture pattern affects the final marine terrace elevations. For the configuration of coupling patches, we refer to previous studies on historical earthquakes for their approximated positions and rupture timings. First, Kanto earthquakes, including Taisho-type earthquakes, which primarily rupture around the Sagami Bay, frequently occur (200–400-year in-

terval), whereas the greater Genroku-type earthquakes infrequently occur, accompanying the rupture beneath the Boso Peninsula (1,200–2,500-year interval) (Shishikura, 2014; Komori et al., 2021). Here, we assign coupling patches to the Taisho-type and Genroku-type ruptures. According to the geodetic investigations, the 1923 Taisho earthquake had two slip concentrations (Sato et al., 2005). We interpret these concentrations as coupling patches and input them into the model as Taisho patches, which release accumulated shear stress every 400 years. Based on the historical records and distribution of the Numa IV terraces, the 1703 Genroku earthquake is estimated to have ruptured beneath the Boso Peninsula (Sato et al., 2016). In addition, geodetic inversion studies have estimated the interplate slip deficit distribution and discovered a coupling beneath the south Boso Peninsula (Sagiya, 2004; Noda et al., 2013). Moreover, tsunami records indicate that the slip area extended to the east by 50–150 km (Matsuda et al., 1978; Yanagisawa and Goto, 2017). Because the Genroku patch shape is more ambiguous than that of the Taisho patches, the forward simulation should include arbitrariness. We set two smaller coupling patches around the south Boso Peninsula to make the moment magnitude of the simulated Genroku event comparable to the previous estimation.

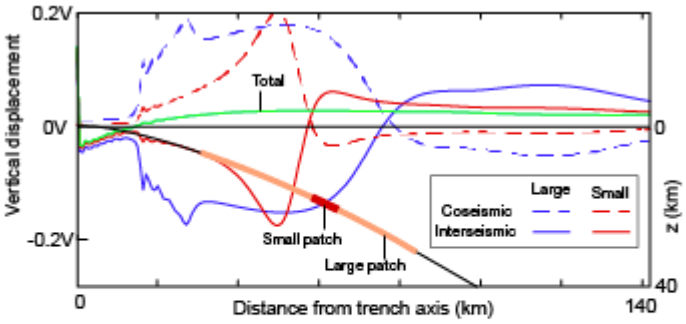

Figure 4. Deformations caused by significantly and partially coupled interfaces. The red and blue extents on the plate interface geometry are the sizes of small and large coupling patches, respectively. The red and blue lines show vertical displacements due to small and large coupling patches, respectively. and the solid and broken lines indicate coseismic and interseismic periods, respectively. The green line represents the total vertical displacement common in both cases.

In addition, we investigate the impact of the coupling patch configuration on the relative heights of marine terraces. The relative heights and formation intervals of the Numa terraces are not linear, which contradicts the kinematic motion because it predicts that the coseismic slip amount is proportional to the waiting time. On the other hand, the mechanical model does not always require a linear relationship between the interval and slip amount because a rupture on a patch affects the stress change on another coupling patch. Therefore, we investigate the vertical deformation history at the southernmost Boso by varying the position and rupture timing of the eastern side of the Genroku patches.

4 Results

4.1. Interplate geometry and long-term deformation

First, we investigated the relationship between the configuration of coupling patches and the long-term deformation. The "long-term" is approximated to the condition when the accumulated shear stress on coupling patches is negligible compared with the total released stress. Therefore, the boundary condition for the long-term case is the following: (1) uniform slip on the steady slip zone and (2) no shear stress change on the coseismic slip area. Figure 4 shows the coseismic, interseismic, and long-term deformations caused by largely and partially coupled slip areas. The variable V indicates the total slip amount on the steady slip zone; the same is applied below. The coseismic and interseismic surface deformations differ significantly, but by canceling each other out, the final deformation distribution is the same.

Figure 5 compares long-term vertical deformation distributions for different plate thicknesses and subducting angles. Permanent subduction is common near the trench axis with broad uplift on the landward side. The parameter study suggested that (1) the steeper the subducting angle, the more localized the uplift near the trough axis, and (2) the thicker the subducting plate, the more uplift remained. These observations are comparable to the demonstration by Kanda and Simons (2010). Although our model is different from Kanda and Simons' settings in the given slip amount on the rupture area, no significant effects were detected because no bump was set on the plate interface in this examination.

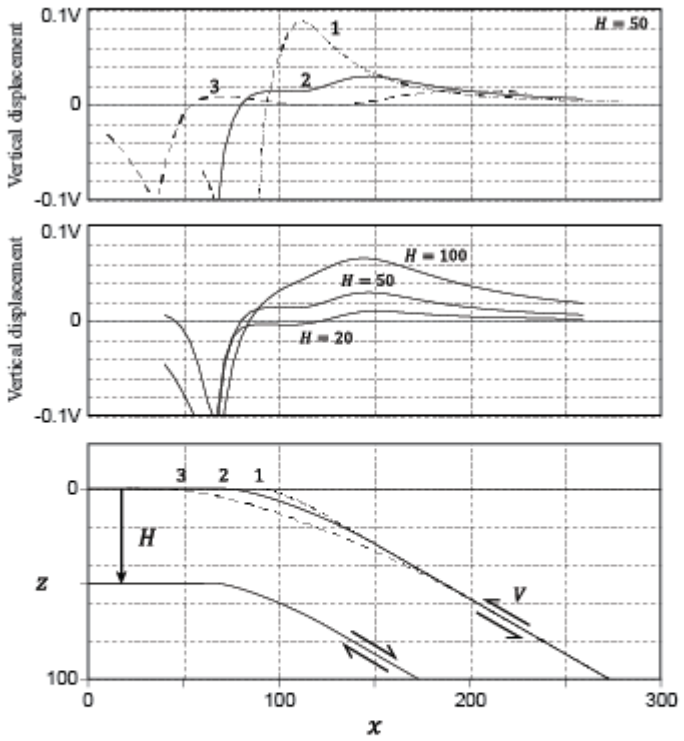

Figure 5. The examination results of the plate thickness and subduction angle. These figures show the geometry and displacements along the trench–normal direction. The bottom panel shows a cross-sectional view of the model geometry. V represents the steady subduction rate. The top and middle panels show the long-term vertical displacement distributions with different subducting angles and thicknesses of the subducting plate H, respectively. The examination of subducting angles uses the plate thickness H=50. The examination of plate thickness uses the intermediate subduction geometry (2 in the bottom panel).

Next, we investigated how a small-scale geometry on the upper plate interface, i.e., a subducted seamount, affects the long-term deformation. Figures 6a and b depict the total slip distribution and vertical surface displacement, respectively, with the plate interface geometry shown as the contour. The total slip amount is approximately comparable to that on the steady slip zone but stalls 10%–15% around the subducted seamount. The permanent uplift is concentrated above the deeper side slope (leading flank) and subsidence above the opposite side (trailing flank). We also evaluated various seamount geometries that are deeper and have a more gradual slope. Figure 6c depicts the cross-sectional profile of the geometry setting and the vertical displacements. The hinge points are consistently above the seamount's summit, but deeper and more gradual seamounts produce gentler deformations.

We also simulated the long-term deformation distribution using the plate interface geometry that models the realistic Sagami Trough subduction zone. Figure

7 shows the depth contour of the modeled upper plate interface of the PHS according to Sato et al. (2005) and Tsumura et al. (2009) (Figure 2a) and the calculated long-term vertical displacement. The realistic geometry model also generates a steep uplift at the southernmost tip of the Boso Peninsula. When we set the total steady slip amount to be 175 m for 7000 years (25 mm/year), the maximum vertical uplift at the southernmost Boso is approximately 30.6 m.

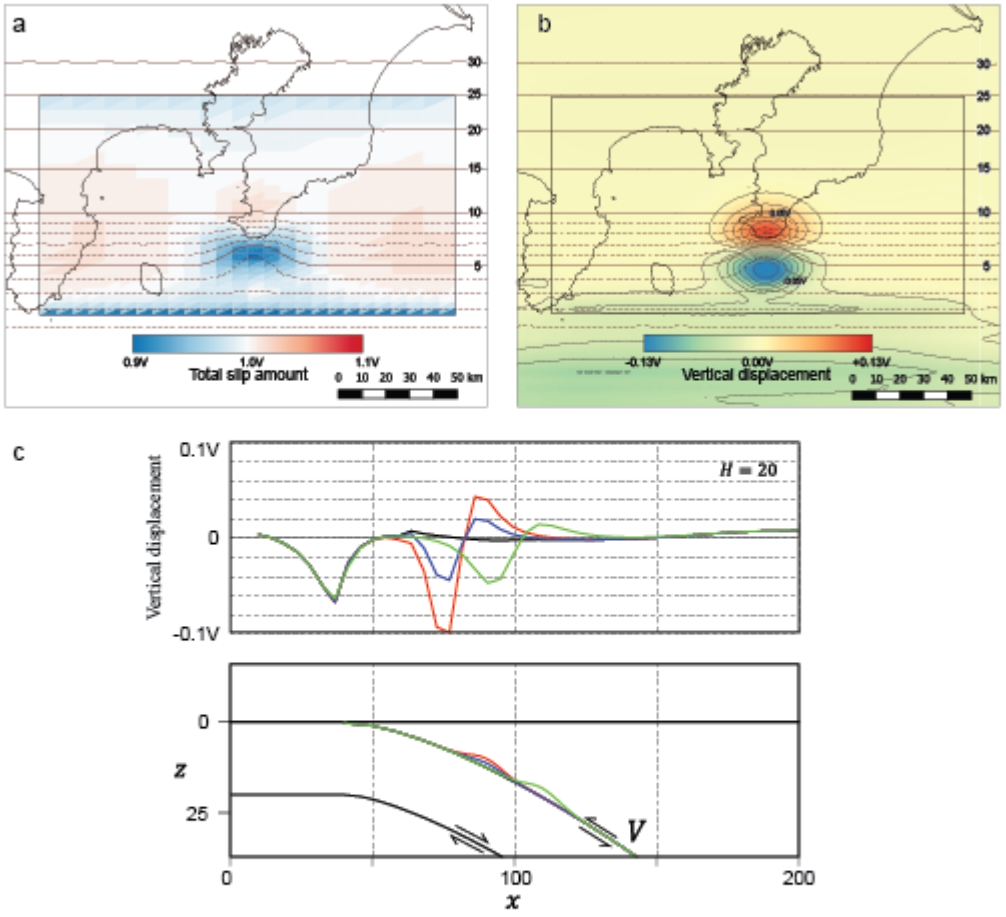

Figure 6. The examination result of the small-scale geometry effect. (a) Total slip distribution on the coseismic slip area. Vrepresents the total slip amount on the steady slip zone. The contour shows the depth of the plate interface, and the unit is a kilometer. (b) The vertical displacement amount on the ground surface. (c) Cross-sectional profiles of the examination results with various interface geometry settings. The top panel depicts the vertical displacement distribution, and the bottom panel depicts the plate interface geometry corresponding to each color. Red: 2 km height at upper part. Blue: 1 km height at upper part. Green: 2 km height at the lower part. Black: No seamount geometry.

4.2.

Rupture delay and the relative heights of marine terraces

Finally, we investigated the effects of the distance and rupture delay of the off-

shore additional coupling patch on the temporal elevation change. Figures 8a and b explain the configuration of the positions and rupture timings of coupling patches. First, the two Taisho patches release shear stress every 400 years, except for the 220-year interval of the last event simulating historical earthquakes. In addition, we fixed the western Genroku patch to rupture at the time of the Numa terrace formation. Then, we tested the relative heights of the simulated Numa terraces by varying the positions and rupture timings of the eastern Genroku patch. Furthermore, we only examine the timing of complementary rupture on the eastern patch to the Numa II event and set it to rupture simultaneously with the western patch at the Numa I, II, and IV events, as shown in Figure 8b.

Figure 8c depicts the time evolution of the elevation change at the southernmost tip of the Boso Peninsula, where the uplift rate is the highest. Four polygonal lines, respectively, indicate the elevation change because each rupture of the western Genroku patch, i.e., the temporal change of the elevation of each Numa terrace level. These lines indicate that the uplifted coastline does not return to sea level in this model, in contrast to the prediction by previous subduction models (Matsu'ura and Sato, 1989; Sato et al., 2016; Noda et al., 2018).

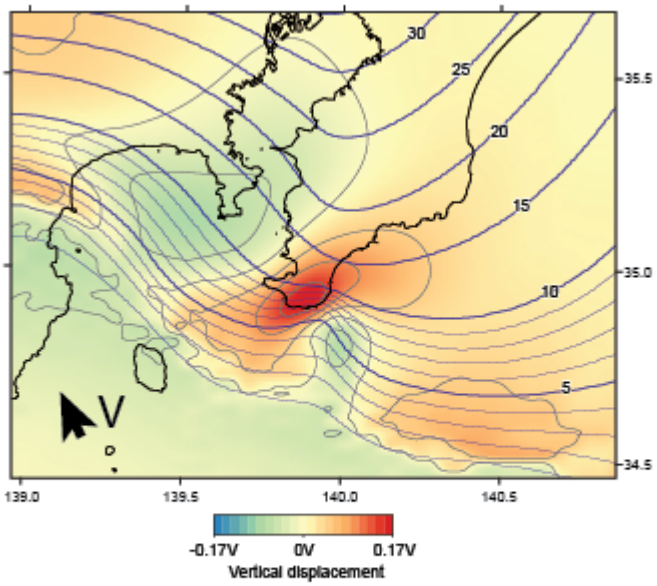

Figure 7. Long-term deformation with the plate interface geometry simulates the realistic Sagami Trough subduction zone. The contour lines indicate the depth (km) of the modeled upper plate interface of the PHS. V represents the total slip amount on the steady slip zone.

Figures 8d and e depict the parameter study results of the eastern Genroku patch. The difference between the largest and smallest relative heights varies up to 0.8 m depending on the position of the eastern Genroku patch. The effect of the eastern patch decreases at 10 km away from the western patch. The relative height difference varies more than 1 m depending on the rupture timing

of the eastern patch. The four Numa terraces show relatively similar relative heights when the eastern patch is closest to the western patch and ruptures 1400 years earlier than the Numa II event.

5 Discussion

5.1 Comparison with geological and geodetic observations

We constructed a rupture scenario using the newly developed mechanical subducting plate model to explain the geological observation. In this investigation, we reproduced the characteristic distributions of Numa terraces, which were not explained by previous kinematic subducting models: the maximum relative heights of 6–7 m and the uplift concentration in the southernmost part of the Boso Peninsula. Previous kinematic models assumed a uniform long-term slip distribution on the plate boundary and regarded the same fault as the sources of coseismic and interseismic deformations (back-slip model). However, this is a strong assumption that was initially proposed to save computational resources and is not universally applicable. In real plate subduction, interseismic deformation arises from the steady slip in a decoupled zone. As a result, the non-uniform slip distribution on the plate interface (Figure 6a) and the asymmetrical deformation pattern between the coseismic and interseismic periods (Figure 4)

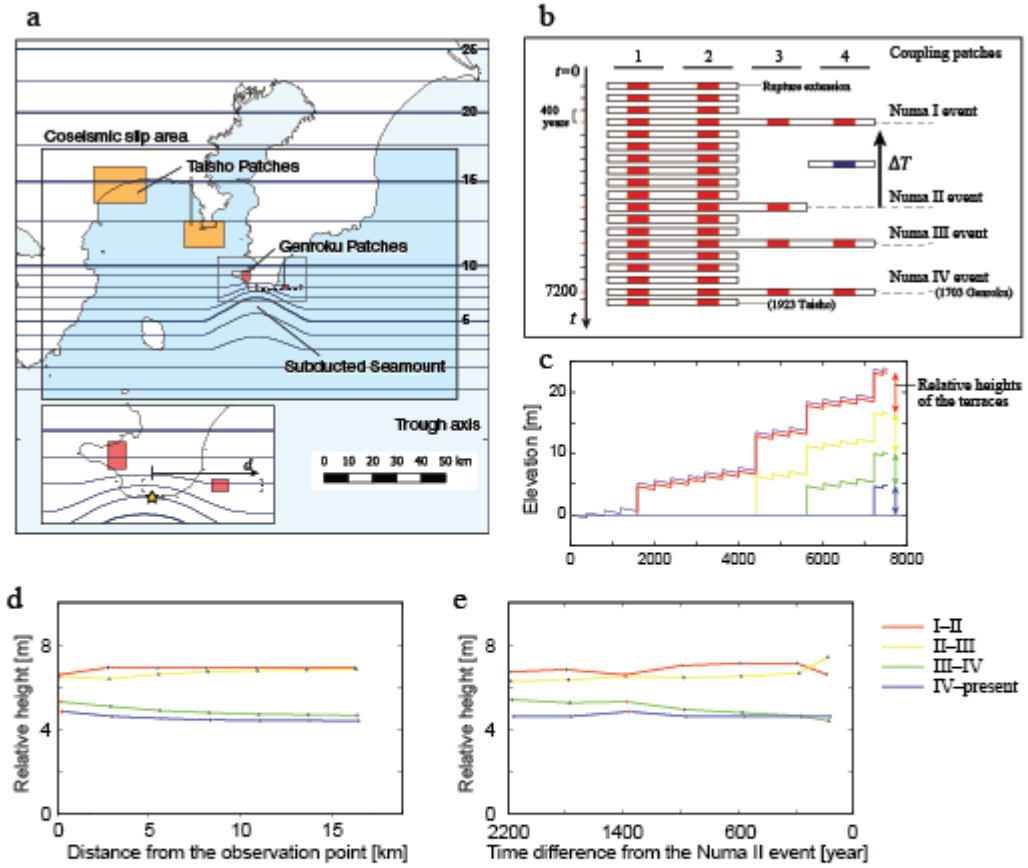

Figure 8. The examination result of the rupture pattern and the elevation of marine terraces. (a) Positions of coupling patches. The eastern part of Genroku patches is adjustable, as examined in (d). (b) Configuration of rupture timings. The rupture timing of patch 4, indicated by the blue rectangle, is adjustable, as examined in (e). (c) Time evolution of the elevation change at the southernmost tip of the Boso Peninsula (yellow circle in (a)). The red, yellow, green, and blue lines represent the elevation change since each rupture of patch 3, as shown in (b). (d and e) Results of the parameter study on the rupture position (d) and timing (e). Each line indicates the relative height of the terrace, indicated by arrows in (c). The result indicated by the red dots is the adopted rupture scenario.

produce

concentrated permanent crustal deformation due to the local interplate geometry (Figures 6b and 7)

Previous studies have also presented other geological and geodetic observations, which we compare with our model's prediction in our rupture scenario and discuss the model's robustness. First, the geodetic observations show the recent crustal deformations in a wider area with higher resolution. Figures 9a and b depict the coseismic vertical displacement of the 1923 Taisho earthquake as measured by the campaign leveling surveys of Land Survey Department (1930) (Miyabe, 1931) and the surface deformation rate as measured by continuous GNSS measurements, from 1/Apr/2004 to 31/Dec/2010, respectively; Figures 9c and d show the simulated counterparts in this model. The complementary

distributions of the interseismic and the 1923 coseismic displacements are well reproduced by our model even though the slip and back-slip amounts are not symmetrical between them. The effect of the subducted seamount is visible in the simulated interseismic surface deformation distribution (Figure 9d), but it is difficult to detect with the current inland observation points. We reproduced the overall features of recent geodetic observations and found that they have less correlation with the long-term deformation pattern.

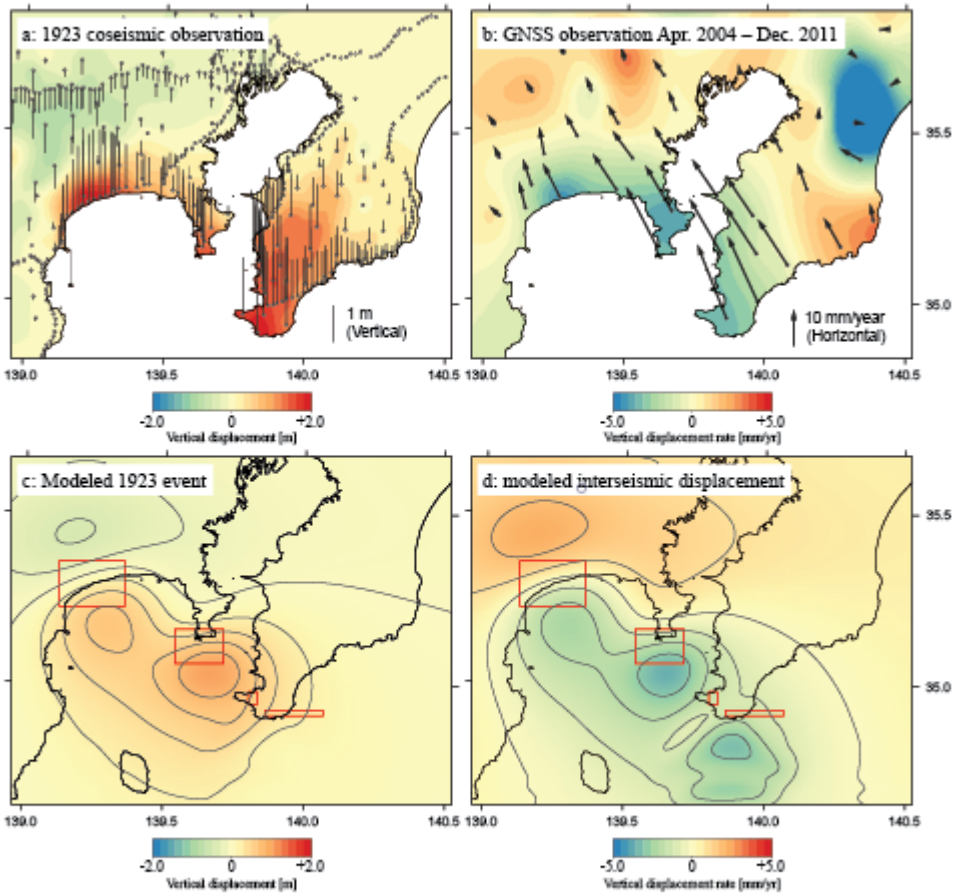

Figure 9. Comparison with geodetic observations. (a) Vertical displacement distribution of the 1923 Taisho earthquake (Miyabe, 1931). (b) Surface deformation rate observed by continuous GNSS measurements. (c) Simulated vertical displacement of the 1923 Taisho earthquake. (d) Simulated surface deformation rate distribution. Red rectangles indicate coupling patches. The steady subduction rate in the simulation is 25 mm/year.

Further analysis to determine the optimal configuration of coupling patches to reproduce these geodetic observations is also possible using the mechanical subducting model. For example, we can create a nonlinear inversion problem by setting the coupling and decoupling on each dislocation mesh as the binary parameter. Sun et al. (2011) created a similar problem. However, such an objective requires a denser meshing and a special calculation setting, which is beyond

the main subject of this study. Moreover, although we set small Genroku coupling patches to adjust the coseismic uplift amount, small coupling patches apply stresses at a higher pace and sooner reach the yield stress. We excluded fracture mechanics in our model but should consider it to develop the model into a comprehensive mechanical model. Therefore, this study only verifies the general correspondence to geodetic observations and leaves these problems to future research. We emphasize that this study did not estimate the optimal positions of the Genroku and Taisho patches.

Previous studies on the 1703 Genroku earthquake source reached a consensus that this event accompanied a large slip to the offshore east (Matsuda et al., 1978; Yanagisawa and Goto, 2017) to explain the tsunami observed along the eastern coast of the Boso Peninsula. This study investigated the contribution of an offshore coupling patch to stress change. However, stress propagation decreases steeply with distance, and the impact was negligible from the estimated tsunami source region (Figure 8). This result indicates the difficulty of estimating the rupture history in the offshore region from coastal and inland deformation even with the mechanical model.

Finally, we compare the simulated long-term deformation pattern (Figure 7) and previous observations. Shishikura (2001) reported that uplifted Holocene seashore deposits are also observed in the middle to the north area of the Boso Peninsula even though there is no uplift in the historical earthquakes (Shishikura, 2014). The mechanical subducting model also explained this inconsistency; the coseismic deformation pattern is mainly affected by the positions of ruptured coupling patches, whereas the long-term deformation pattern depends on the plate interface geometry. Therefore, the highest Holocene marine terrace is distributed in a broader area than the coseismic uplift. The simulated long-term deformation distribution (Figure 7) in this study also produced a broad uplift on the hanging wall. We note that this model shows a gently subsiding area around the Miura Peninsula even though a long-term uplift trend is estimated in the Miura Peninsula from Holocene and Pleistocene marine terraces (Ota et al., 1994). This modeled subsidence is probably caused by the bending around the Izu Peninsula. However, the Izu Peninsula marks a land collision and is not estimated to subduct steadily in reality (Hashimoto and Terakawa, 2018). As a result, the western part of the Sagami Trough needs additional constraints to simulate a more realistic deformation pattern.

The proposed mechanical subducting model simulated a more realistic feature of plate subduction than previous observations. However, we still ignore other physical configurations for simplification. Here, we note factors that possibly impact the results and evaluate their effects. First, we simulated the subduction in an elastic half-space and excluded the viscoelastic effect in the asthenosphere. We focused on the deformation process of 400–10,000 years, which is significantly longer than the stress relaxation time (~5 years) for a typical value of asthenosphere viscosity (Matsu'ura and Iwasaki, 1983; Sato et al., 2016) and even the complete post-seismic decay of the transient vertical displacement (>100 years)

(Sato and Matsu'ura, 1988). Along with the asthenospheric flow, gravitational compensation (Matsu'ura et al., 1989) is also excluded. This effect is because the stress relaxation assumes the slip and back-slip sequences in elastic/viscoelastic layers and cannot simply be compared with the proposed model. However, this deformation depends on the large-scale plate interface geometry comparable to that in this study (Figure 6) and can be discussed separately from the contribution from the subducted seamount.

Moreover, the accumulated stress on the slip area is not entirely released after the earthquake sequences in this model. First, we calculated only the direction parallel to the plate subduction direction for simplification and thus neglected the stress accumulation perpendicular to that. A winding plate boundary can also load the shear stress in this direction, which may slightly impact the result. We did not investigate the perpendicular slip because this study's purpose is satisfied with the first-order approximation. Nevertheless, future studies with higher resolution observation will be required to include it. Finally, we should note the accumulation of the normal stress on the plate interface. Intuitively, a concentration of the normal stress on the leading flank of the subducted seamount can be estimated. This accumulation is not released by the slip parallel to the interface and thus considerably remained after the earthquake sequences. In practice, this normal stress is probably released by the plastic yielding within the upper plate, as observed by analog experiments (Dominguez et al., 1998; 2000). However, this process takes a significantly longer time scale than the earthquake recurrence at the plate interface. As previously mentioned, the structural surveys did not detect any intraplate faulting in the upper plate around the survey area (Sato et al., 2006; Miura et al., 2009; Tsumura et al., 2009). Therefore, we assume that the accumulation of the normal stress persists on the plate interface along the Sagami Trough and include the remaining stress in the simulation.

5.2 Re-evaluation of the Kanto earthquakes

By investigating the geological and geomorphological observations (Komori et al., 2020; 2021) using the mechanically consistent model, we proposed a rupture scenario of the Kanto earthquakes for more than 6,000 years. Conventionally, the Kanto earthquakes have been regarded as a recurrence of the smaller Taisho-type earthquakes and the greater Genroku-type earthquakes that uplifted the Numa terraces. However, this study demonstrated that partitioning the eastern coupling patches of the Genroku earthquakes and the rupture delay in the past event is required to explain the present coastal landform. The proposed scenario in this study is not a unique solution to the observation but at least indicates that the traditionally accepted periodic rupture pattern (i.e., characteristic earthquakes) cannot reproduce the present distribution of the Numa terraces.

Moreover, we did not discuss the rupture to the east offshore, the tsunami source region of the 1703 Genroku event. Regarding the spatiotemporal rupture variation of the Genroku patch, this region can have various rupture pat-

terns, including a single rupture on the offshore patch. This study suggested that it is difficult to retrieve the rupture history of the offshore patch from the inland surface deformation record. Therefore, the investigation of the tsunami deposits and historical records along the eastern coast of the Kanto region also has significant importance for hazard assessment.

5.3 Comparison with previous deformation models

This study connected the earthquake recurrence and the geological observation of the marine terraces using a physically consistent crustal deformation model for the first time. Finally, we summarize the difference between earthquake recurrence models using mechanical and kinematic boundary conditions. First, the fundamental differences between them arise from the assumption of the coseismic slips; kinematic models impose the coseismic slip to cancel out the interseismic back-slip, whereas our mechanical model determines the coseismic slip by releasing the accumulated shear stress. This mechanical boundary condition results in the asymmetrical coseismic slip with the amount of the interseismic plate motion (kinematically assumed back-slip), where the back-slip on the fault does not cancel out the coseismic slip. Besides, the long-term deformation distribution is not simply the summation of the coseismic displacement in both models.

We would emphasize the importance of local geometrical irregularity, such as the seamount discussed. Conventional kinematic models ignore the effect of the permanent slip on the deformation (Savage, 1983), but this assumption is valid only for a planar plate interface, as highlighted by Matsu'ura et al. (1989). Furthermore, Romanet et al. (2020) demonstrated that the deformation increases as the curvature of the fault increases. In this sense, the surface displacement patterns can depend on local bumps at the plate interface.

We note the interpretation by Sato et al. (2016) and Noda et al. (2018) about the formation process of the Numa terraces using the kinematic deformation model. Sato et al. (2016) suggested that "it would not be a reliable way to estimate the recurrence interval of the Genroku-type events from the difference in age between adjoining terraces" because "the coseismic vertical displacement pattern gradually fades out with time, and after the completion of one earthquake cycle, only a permanent displacement due to steady plate subduction remains." Although the interseismic back-slip will cancel out the coseismic displacement in their model, the amount of the interseismic subsidence is less than the coseismic uplift caused by the amount of the relative plate motion during the interseismic period, retaining the permanent uplift. This means that the uplifted terrace will not return to sea level, even in their model. This feature is shared by our model even though both models differ in the boundary condition, as discussed above. In such a condition, we can naturally expect stairs such as topography to be retained after several cycles. In conclusion, we cannot directly compare the relative terrace height with the coseismic uplift without properly correcting the interseismic subsidence; however, we can correlate terrace formation ages with the timings of uplift events more easily.

6 Conclusion

We examined the spatiotemporal crustal deformation around the subduction zone using the newly proposed mechanical earthquake recurrence model. The novel mechanical subducting plate model comprises the recurrence of steady loading in the interseismic period and coseismic stress release, which can produce asymmetric slip distributions between the interseismic and coseismic periods. Previous kinematic subducting models have assumed that the interseismic and coseismic slips cancel each other out and underestimated the contribution from the local interplate geometry, such as subducted seamounts. The Numa terraces, located in the southernmost part of the Boso Peninsula, have a unique distribution in which the elevations decrease significantly more steeply than the prediction from the effect of plate bending at a subduction zone (Sato and Matsu'ura 1988; Kanda and Simons, 2010). We simulated the plate boundary that includes the shape of the subducted seamount (Tsumura et al., 2009) and indicated that a local bump could produce short-wavelength permanent surface uplift. The simulated uplift rate at the southernmost tip of the Boso Peninsula was 4 mm/year and was comparable to the elevation of Numa I (25–30 m uplift in 5,800 years). In addition, the uplift rate at the middle part of the Boso Peninsula was also consistent with the elevation of the detected highest Holocene marine deposits (Shishikura, 2014), which did not correlate with the coseismic deformations.

Moreover, the mechanical model allows us to discuss the coseismic deformation and rupture recurrence, along with the long-term deformation, in a single simulation. We placed coupling patches on the Sagami Trough plate interface and reproduced the Holocene earthquake recurrence. Although the four levels of Numa terraces recorded the recurrence of the greater Genroku-type earthquakes, previous kinematic models could not sufficiently explain their formation process because their elevations and formation ages were not linear. This study investigated the effect of the positions and rupture delay of coupling patches and demonstrated a rupture scenario with variable rupture patterns. Finally, we proposed a rupture scenario to reproduce the elevations of the Numa terraces. The findings also indicate that the similarity in the spatial distribution of the marine terraces does not directly imply the similarity in the rupture of the source earthquakes.

The essential improvement in the subduction model employing mechanical coupling is the inclusion of the effect of the local interplate geometry on the total slip and deformation distributions. Because previous kinematic subducting models have frequently assumed a back-slip model and a uniform slip on the plate boundary, the contribution from the interplate geometry has been underestimated despite being observed in geomorphological studies and analog experiments. We highlighted that the non-uniform long-term slip and asymmetrical deformation distributions caused by the local interplate geometry derived from the mechanical subducting model can produce local variable permanent crustal deformations.

These findings strongly impact the estimation of past earthquake recurrences using coastal landforms. For example, we believe that the compilation of similar marine terrace distributions will reveal similar-sized megathrust earthquakes with similar intervals (i.e., characteristic earthquakes). However, this study demonstrated that variable sizes and intervals of earthquakes could produce similar distributions of marine terraces. Therefore, simplifying assumptions for the marine terrace formation and earthquake histories could lead to underestimation or overestimation in future hazard assessments. A comprehensive geological dataset, well-constrained interplate geometry, and physically consistent modeling are critical to deconvolute the present elevations of the marine terraces into individual rupture events.

Acknowledgments

The MCS reflection data shown in Figure 2b can be requested through JAMSTEC Seismic Survey Database (https://doi.org/10.17596/0002069). The topography data used in Figures 1 and 2a are the 30-arc sec General Bathymetric Chart of the Oceans (GEBCO) data (The GEBCO_2022 Grid). We used the DEM Viewer Blender application for the visualization of Figure 2a (https://doi.org/10.5281/zenodo.7091899). The authors would like to thank Enago (www,enago.jp) for the English language review. This study was supported by the Ministry of Education, Culture, Sports, Science and Technology (MEXT) of Japan, under its Earthquake and Volcano Hazards Observation and Research Program.

References

Dominguez, S., Lallemand, S. E., Malavieille, J., von Huene, R., (1998). Upper plate deformation associated with seamount subduction, *Tectonophysics*, **293**, 207–224. https://doi.org/10.1016/S0040-1951(98)00086-9

Dominguez, S., Malavielle, J., Lallemand, S. E. (2000). Deformation of accretionary wedges in response to seamount subduction- Insights from sandbox experiments, *Tectonics*, **19**, 182–196. https://doi.org/10.1029/1999TC900055

Fujiwara, O., Masuda, F., Sakai, T., Irizuki, T., Fuse, K. (2000). Tsunami deposits in Holocene bay mud in southern Kanto region, Pacific coast of central Japan, *Sedimentary Geology*, **135**, 219–230.
https://doi.org/10.1016/S0037-0738(00)00073-7

Fukahata, Y., Matsu'ura, M. (2016). Deformation of island-arc lithosphere due to steady plate subduction. *Geophysical Journal International*, **204**, 825–840.
https://doi.org/10.1093/gji/ggv482

Gardner, T., Marshall, J., Merritts, D., Bee, B., Burgette, R., Burton, E., et al. (2001). Holocene forearc block rotation in response to seamount subduction, southeastern Península de Nicoya, Costa Rica, *Geology*, **29**, 151–154.
https://doi.org/10.1130/0091-7613(2001)029<0151:HFBRIR>2.0.CO;2

Grant, L.B., Sieh, K. (1994). Paleoseismic evidence of clustered earthquakes on

the San Andreas Fault in the Carrizo Plain, California. *Journal of Geophysical Research*, **99**, 6819e6841. https://doi.org/10.1029/94JB00125.

Hashimoto C., Fukui K., Matsu'ura M. (2004). 3-D modelling of plate interfaces and numerical simulation of long-term crustal deformation in and around Japan. *Pure and Applied Geophysics*, **161**, 2053–2068, https://doi.org/10.1007/s00024-004-2548-8

Hashimoto, C., Terakawa, T. (2018). Stress data inversion to estimate collision rate distribution and its application to the Izu Peninsula, Japan. *Tectonophysics*. **744**, 47–57. https://doi.org/10.1016/j.tecto.2018.06.001

Herman, M. W., Furlong, K. P., Govers, R. (2018). The accumulation of slip deficit in subduction zones in the absence of mechanical coupling: Implications for the behavior of megathrust earthquakes. *Journal of Geophysical Research: Solid Earth*, 123, 8260–8278. https://doi.org/10.1029/2018JB016336

Herman, M. W., Govers, R. (2020). Locating fully locked asperities along the South America subduction megathrust: A new physical interseismic inversion approach in a Bayesian framework. *Geochemistry, Geophysics, Geosystems*, **21**, e2020GC009063. https://doi.org/10.1029/2020GC009063

Hirose, F., Nakajima, J., Hasegawa, A. (2008) Three-dimensional velocity structure and configuration of the Philippine Sea slab beneath Kanto District, central Japan, estimated by double-difference tomography: *Zisin*, **60**, p. 128–138, https://doi.org/10.4294/zisin.60.123 (in Japanese with English abstract).

Johnson, K. M., Segall, P. (2004). Viscoelastic earthquake cycle models with deep stress-driven creep along the San Andreas fault system. *Journal of Geophysical Research*, **109**, B10403, https://doi:10.1029/2004JB003096

Johnson, K. M., Fukuda, J. (2010), New methods for estimating the spatial distribution of locked asperities and stress-driven interseismic creep on faults with application to the San Francisco Bay Area, California, *Journal of Geophysical Research*, **115**, B12408, https://doi.org/10.1029/2010JB007703.

Kanda, R. V. S., Simons, M. (2010). An elastic plate model for interseismic deformation in subduction zones, *Journal of Geophysical Research*, **115**, B03405, https://doi.org/10.1029/2009JB006611

Kanda, R. V. S., Simons, M. (2012). Practical implications of the geometrical sensitivity of elastic dislocation models for field geologic surveys, *Tectonophysics*, **560–561**, 94–104. https://doi.org/10.1016/j.tecto.2012.06.040

Kawakami, S., Shishikura, M. (2006). Geological Map 1:50,000. Tateyama, Geological Survey of Japan, (in Japanese with English abstract).

Keller, E.A., Pinter, N. (2002). Active tectonics: earthquakes, uplift, and landscape. Prentice-Hall, Upper Saddle River.

Komatsubara, T. (2017). Some facts on activity of southern part of the Kamogawa Lowland fault zone, Boso peninsula, central Japan, Ac-

tive Fault Research, 46, 17–25. (in Japanese with English abstract). https://doi.org/10.11462/afr.2017.46_17

Komori, J., Shishikura, M., Ando, R., Yokoyama, Y., Miyairi, Y. (2017). History of the great Kanto earthquakes inferred from the ages of Holocene marine terraces revealed by a comprehensive drilling survey. *Earth and Planetary Science Letters*, **471**, 74–84. https://doi.org/10.1016/j.epsl.2017.04.044

Komori, J., Ando, R., Shishikura, M. (2020). Cluster analysis of marine terraces and quantitative seismotectonic interpretation of the Boso Peninsula, central Japan. *Journal of Geophysical Research: Solid Earth*, **125**, e2019JB019211. https://doi.org/10.1029/2019JB019211

Komori, J., Shishikura, M., Ando, R., Yokoyama, Y., Miyairi, Y. (2021). The history of the great Kanto earthquakes, central Japan: A Bayesian approach to age estimation of marine terraces. *Quaternary Science Reviews*, **272**, 107217, https://doi.org/10.1016/j.quascirev.2021.107217

Land Survey Department (1930). Re-survey of the Kwanto district after the great earthquake of 1923, *Bulletin of the Imperial Earthquake Investigation Committee*, **11**, 1–6.

Lindsey, E.O., Mallick, R., Hubbard, J.A., Hubbard, J. A., Bradley, K. E., Almedia, R. V., Moore, J. D. P., et al. (2021). Slip rate deficit and earthquake potential on shallow megathrusts. *Nature Geoscience*. **14**, 321–326. https://doi.org/10.1038/s41561-021-00736-x

Litchfield, N. J., Ellis, S., Berryman, K., Nicol, A. (2007). Insights into subduction-related uplift along the Hikurangi Margin, New Zealand, using numerical modeling. *Journal of Geophysical Research: Earth Surface*, **112**, F02021, https://doi.org/10.1029/2006JF000535

Litchfield, N. J., Clark, K. J., Cochran, U. A., Palmer, A. S., Mountjoy, J., Mueller, C., et al., (2020). Marine terraces reveal complex near-shore upper-plate faulting in the northern Hikurangi margin, New Zealand. *Bulletin of the Seismological Society of America*, **110**, 825–849, https://doi.org/10.1785/0120190208

Matsuda, T., Ota, Y., Ando, M., Yonekura, N. (1978). Fault mechanism and recurrence time of major earthquakes in southern Kanto district, Japan, as deduced from coastal terrace data. *Geological Society of America Bulletin*, **89**, 1610-1618. https://doi.org/10.1130/0016-7606(1978)89%3C1610:FMARTO%3E2.0.CO;2

Matsu'ura, M, Sato, T. (1989). A dislocation model for the earthquake cycle at convergent plate boundaries. Geophysical Journal International, **96**, 23–32, https://doi.org/10.1111/j.1365-246X.1989.tb05247.x

Miura, S., Yamashita, M., Takahashi, N., No, T., Kodaira, S., Nozaki, K., Kobayashi, R. (2009). Multichannel seismic profiles crossing source regions of

megathrust earthquakes and slow slip events off-Boso, central Japan, American Geophysical Union 2009 Fall Meeting, NH31A-1093

Miyabe, N. (1931). On the vertical earth movements in Kwanto districts, *Bulletin of Earthquake Research Institute, the University of Tokyo*, **9**, 1-21. http://hdl.handle.net/2261/9977

Nishimura, T., Hirasawa, T., Miyazaki, S., Sagiya, T., Tada, T., Miura, S., Tanaka, K. (2004). Temporal change of interplate coupling in northeastern Japan during 1995–2002 estimated from continuous GPS observations. *Geophysical Journal International*, **157**, 901–916. https://doi.org/10.1111/j.1365-246X.2004.02159.x

Nakata, T., Koba, M., Imaizumi, T., Jo, W., Matsumoto, H. Suganuma, T. (1980). Holocene marine terraces and seismic crustal movements in the southern part of Boso Peninsula, Kanto, Japan. *Geographical Review of Japan, Series A*, **53**, 29-44, (in Japanese with English abstract and figure captions). https://doi.org/10.4157/grj.53.29

Noda, A., Hashimoto, C., Fukahata, Y., Matsu'ura, M. (2013). Interseismic GPS strain data inversion to estimate slip-deficit rates at plate interfaces: application to the Kanto region, central Japan, *Geophysical Journal International*, **193**, 61–77, https://doi.org/10.1093/gji/ggs129

Noda, A., Miyauchi, T., Sato, T., Matsu'ura, M. (2018). Modelling and simulation of Holocene marine terrace development in Boso Peninsula, central Japan. *Tectonophysics*, **731**, 139–154. https://doi.org/10.1016/j.tecto.2018.03.008

Ota, Y., Fujimori, T., Kashima, K., Kanie, Y., Matsushima, Y. (1994). Data on Holocene Marine Terraces at the Eastern Margin of Kitatake Fault, Miura Peninsula, South Kanto. *The Quaternary Research (Daiyonki Kenkyu).* **33**, 37–43. (in Japanese). https://doi.org/10.4116/jaqua.33.37

Philibosian, B., Meltzner, A. J. (2020). Segmentation and supercycles: A catalog of earthquake rupture patterns from the Sumatran Sunda Megathrust and other well-studied faults worldwide. *Quaternary Science Reviews*, **241**, 106390. https://doi.org/10.1016/j.quascirev.2020.106390

Plafker, G. (1969). Tectonics of the March 27, 1964 Alaska earthquake: U.S. Geological Survey Professional Paper 543–I, 74 p., 2 sheets, scales 1:2,000,000 and 1:500,000. https://pubs.usgs.gov/pp/0543i/

Ramos N. T., Tsutsumi, H. (2010). Evidence of large prehistoric offshore earthquakes deduced from uplifted Holocene marine terraces in Pangasinan Province, Luzon Island, Philippines. *Tectonophysics*, **495**, 145–158. https://doi.org/10.1016/j.tecto.2010.08.007

Romanet, P., Sato, D. S. K., Ando, R. (2020). Curvature, a mechanical link between the geometrical complexities of a fault: application to bends, kinks and rough faults. *Geophysical Journal International*, **223**, 211–232. https://doi:10.1093/gji/ggaa308

Sagiya, T. (2004). Interplate coupling in the Kanto District, central Japan, and the Boso Silent earthquake in May 1996, *Pure and Applied Geophysics*, **161**, 11-12, 2601-2616. https://doi.org/10.1007/s00024-004-2566-6

Sato, H., Hirata, N., Koketsu, K., Okaya, D., Abe, S., Kobayashi, R., et al. (2005). Earthquake source fault beneath Tokyo. *Science*, **309**, 462–464. DOI: 10.1126/science.1110489

Sato, T., Matsu'ura, M. (1988) A kinematic model for deformation of the lithosphere at subduction zones, *Journal of Geophysical Research*, **93**, 6410–6418. https://doi.org/10.1029/JB093iB06p06410

Sato, T., Higuchi, H., Miyauchi, T., Endo, K., Tsumura, N., Ito, T., et al. (2016). The source model and recurrence interval of Genroku-type Kanto earthquakes estimated from paleo-shoreline data. *Earth, Planets and Space*, **68**, 1–17. https://doi.org/10.1186/s40623-016-0395-3

Savage, J. C. (1983). A dislocation model of strain accumulation and release at a subduction zone. *Journal of Geophysical Research*, **88**, 4984–4996. https://doi.org/10.1029/JB088iB06p04984

Shimazaki, K., Nakata, T. (1980). Time-predictable recurrence model for large earthquakes. *Geophysical Research Letters*, **7**, 279–282. https://doi.org/10.1029/GL007i004p00279

Shishikura, M., Haraguchi, T., Miyauchi, T. (2001). Timing and recurrence interval of the Taisho-type Kanto Earthquake, analyzing Holocene emerged shoreline topography in the Iwai Lowland, the southwestern part of the Boso Peninsula, central Japan, *Zisin 2*, **53**, 357-372, (in Japanese with English abstract and figure captions). https://doi.org/10.4294/zisin1948.53.4_357

Shishikura, M. (2014). History of the paleo-earthquakes along the Sagami Trough, central Japan: Review of coastal paleo-seismological studies in the Kanto region. *Episodes*, **37**, 246–257. https://doi.org/10.18814/epiiugs/2014/v37i4/004

Sun, J., Johnson, K. J., Cao, Z., Shen, Z., Bürgmann, R., Xu, X. (2011). Mechanical constraints on inversion of coseismic geodetic data for fault slip and geometry: Example from InSAR observation of the 6 October 2008 Mw 6.3 Dangxiong-Yangyi (Tibet) earthquake. *Journal of Geophysical Research: Solid Earth*, **116**, B01406, https://doi.org/10.1029/2010JB007849

Tsumura, N., Komada, N., Sano, J., Kikuchi, S., Yamamoto, S., Ito, T., et al. (2009). A bump on the upper surface of the Philippine Sea plate beneath the Boso Peninsula, Japan inferred from seismic reflection surveys: A possible asperity of the 1703 Genroku earthquake. *Tectonophysics*, **472**, 39–50. https://doi.org/10.1016/j.tecto.2008.05.009

Usami, T., Ishi, H., Imamura, T., Takemura, M., Matsuura, R. (2013). Materials for comprehensive list of destructive earthquakes in Japan. Univ. Tokyo Press (in Japanese).

Wang, Y., Shyu, J.B.H., Sieh, K., Chiang, H.-W., Wang, C.-C., Aung, T., et

al. (2013). Permanent upper plate deformation in western Myanmar during the great 1762 earthquake: Implications for neotectonic behavior of the northern Sunda megathrust. *Journal of Geophysical Research: Solid Earth*, **118**, 1277-1303. 10.1002/jgrb.50121

Watanabe, A. (1929). Preliminary Note on the Coastal Terraces of the Southern Parts of Bôsô Peninsula, *Geographical review of Japan*, **5**, 119–126. https://doi.org/10.4157/grj.5.119

Yanagisawa, H., Goto, K. (2017) Source model of the 1703 Genroku Kanto earthquake tsunami based on historical documents and numerical simulations: modeling of an offshore fault along the Sagami Trough. *Earth Planets, and Space*, **69**, 136. https://doi.org/10.1186/s40623-017-0713-4

Yoshioka, S., Yabuki, T., Sagiya, T., Tada, T., Matsu'ura, M. (1993). Interplate coupling and relative plate motion in the Tokai district, central Japan, deduced from geodetic data inversion using ABIC. *Geophysical Journal International*, **113**, 607–621. https://doi.org/10.1111/j.1365-246X.1993.tb04655.x

Figure 1. Survey region of this study and geological observations. (a) Tectonic setting of the Sagami Trough. The red meshed area indicates the estimated source region of historical Kanto earthquakes (Sato et al., 2005; Sato et al., 2016). The red triangles indicate Quaternary volcanoes (Nakano et al., 2013). (c) Distribution of Numa terraces following Komori et al. (2020).

Figure 2. (a) Bathymetry map around the survey region and the profile lines of previous reflection surveys (Sato et al., 2005; Kimura et al., 2009; Miura et al., 2009; Tsumura et al., 2009). The blue contour lines indicate the estimated depth of the upper PHS by Tsumura et al. (2009). (b) Post stack time-migrated reflection image of the BOS-1C profile (Miura et al., 2009). The solid black line represents our interpretation of the plate interface. Triangles indicate the positions of intersections with the survey lines of Tsumura et al. (2009).

Figure 3. Schematic illustration of the mechanical plate subduction model. The boundary conditions during the interseismic period are displayed in this figure. The steady slip zone is given as a sufficiently large area compared with the coseismic slip area in the model even though it is excluded in this figure.

Figure 4. Deformations caused by significantly and partially coupled interfaces. The red and blue extents on the plate interface geometry are the sizes of small and large coupling patches, respectively. The red and blue lines show vertical displacements due to small and large coupling patches, respectively. and the solid and broken lines indicate coseismic and interseismic periods, respectively. The green line represents the total vertical displacement common in both cases.

Figure 5. The examination results of the plate thickness and subduction angle. These figures show the geometry and displacements along the trench–normal direction. The bottom panel shows a cross-sectional view of the model geometry.

V represents the steady subduction rate. The top and middle panels show the long-term vertical displacement distributions with different subducting angles and thicknesses of the subducting plate H, respectively. The examination of subducting angles uses the plate thickness $H = 50$. The examination of plate thickness uses the intermediate subduction geometry (2 in the bottom panel).

Figure 6. The examination result of the small-scale geometry effect. (a) Total slip distribution on the coseismic slip area. Vrepresents the total slip amount on the steady slip zone. The contour shows the depth of the plate interface, and the unit is a kilometer. (b) The vertical displacement amount on the ground surface. (c) Cross-sectional profiles of the examination results with various interface geometry settings. The top panel depicts the vertical displacement distribution, and the bottom panel depicts the plate interface geometry corresponding to each color. Red: 2 km height at upper part. Blue: 1 km height at upper part. Green: 2 km height at the lower part. Black: No seamount geometry.

Figure 7. Long-term deformation with the plate interface geometry simulates the realistic Sagami Trough subduction zone. The contour lines indicate the depth (km) of the modeled upper plate interface of the PHS. V represents the total slip amount on the steady slip zone.

Figure 8. The examination result of the rupture pattern and the elevation of marine terraces. (a) Positions of coupling patches. The eastern part of Genroku patches is adjustable, as examined in (d). (b) Configuration of rupture timings. The rupture timing of patch 4, indicated by the blue rectangle, is adjustable, as examined in (e). (c) Time evolution of the elevation change at the southernmost tip of the Boso Peninsula (yellow circle in (a)). The red, yellow, green, and blue lines represent the elevation change since each rupture of patch 3, as shown in (b). (d and e) Results of the parameter study on the rupture position (d) and timing (e). Each line indicates the relative height of the terrace, indicated by arrows in (c). The result indicated by the red dots is the adopted rupture scenario.

Figure 9. Comparison with geodetic observations. (a) Vertical displacement distribution of the 1923 Taisho earthquake (Miyabe, 1931). (b) Surface deformation rate observed by continuous GNSS measurements. (c) Simulated vertical displacement of the 1923 Taisho earthquake. (d) Simulated surface deformation rate distribution. Red rectangles indicate coupling patches. The steady subduction rate in the simulation is 25 mm/year.

Appendix

We formulate the governing equation and boundary conditions of the mechanical subducting plate model and earthquake recurrence. We use the static boundary element method with the triangular element embedded in a homogeneous elastic half-space (Meade, 2007). The shear stress change on an element, $\Delta\tau$, and the displacement on the surface, Δu, caused by dislocation on an element, s, are given by the representation theorem:

$$\Delta\tau_i = \Sigma_j K_{\mathrm{ij}}^{\mathrm{trac}} s_j, \quad \text{(A1)}$$

$$\Delta u_i = \Sigma_j K_{\mathrm{ij}}^{\mathrm{disp}} s_j, \quad \text{(A2)}$$

where K^{trac} and K^{disp} denote the kernel matrices, and i and j denote the index numbers of the receiver point and the source element, respectively. The shear stress change is calculated at the center of gravity of each triangle element.

Next, we construct the boundary conditions assigned to the aseismic and seismic areas in the interseismic and coseismic periods. The upper plate boundary is divided into a steady slip zone and a coseismic slip area. The coseismic slip area consists of coupling patches and the remaining decoupled zone. For the interseismic period, we first apply a uniform slip V to the lower plate boundary and the steady slip zone on the upper boundary. The slip directions on the upper and lower boundaries should be opposite. On the coseismic slip area, the mixed boundary conditions are given:

$$s_{i\in(\text{coupling patch})} = 0, \quad \text{(A3)}$$

$$\Delta\tau_{i\in(\text{decoupled zone})} = 0. \quad \text{(A4)}$$

The solution for the boundary condition of stress (equation A4) is given by

$$s_i = \Sigma_j \left(K^{\mathrm{trac}}\right)^{-1}_{\mathrm{ij}} \Delta\tau_j, \quad \text{(A5)}$$

where $\left(K^{\mathrm{trac}}\right)^{-1}$ denotes the inversion matrix of K^{trac}. This equation allows us to calculate the shear stress change in the coseismic slip area throughout the interseismic period.

For the coseismic slip, we first prepare the stress drop distribution $\Delta\tau'$, which is the sum of interseismic stress changes and the inherited accumulated stress from the preceding cycle. We use the other mixed boundary conditions to calculate the coseismic slip:

$$\Delta\tau_{i\in(\text{rupture area})} = -\Delta\tau_i^{'} \quad \text{(A6)}$$

$$s_{i\in(\text{intact area})} = 0, \quad \text{(A7)}$$

where the rupture area includes the decoupled zone and the designated coupling patches to rupture, and the intact area means the remaining coupling patches. At the coseismic event, the shear stress is accumulated on the intact area and is passed to the next event.